Influences of temperature-dependent thermal conductivity on surface heat flow near major faults

Byung-Dal So[1] and David A. Yuen[2,3,4]

Received 18 June 2013; revised 18 July 2013; accepted 19 July 2013; published 12 August 2013.

[1] We studied the thermomechanical effects on surface heat flow near major faults from positive feedback between temperature-dependent thermal conductivity $k(T) \propto (1/T)^b$ and frictional heating in a crust-lithosphere system using finite element simulations. Variable conductivity and frictional heating cause a drastic reduction in the thermal conductivity, and these changes can impact the heat flux. When $b = 1$, the temperature is 400 K higher around the fault than in the uniform conductivity case. This is caused by the reduction in thermal conductivity. In spite of the high temperature around the fault in the variable conductivity cases, the surface heat flux is 30% (for $b = 0.5$) to 50% (for $b = 1$) lower than in the uniform conductivity case. This thermal insulating effect may explain the lack of heat flow anomalies near major faults and is consistent with previous hypotheses about the nature of the shear strength associated with these faults. **Citation:** So, B.-D., and D. A. Yuen (2013), Influences of temperature-dependent thermal conductivity on surface heat flow near major faults, *Geophys. Res. Lett.*, *40*, 3868–3872, doi:10.1002/grl.50780.

1. Introduction

[2] Surface heat flow is one of the most important geophysical constraints to understand the thermal-mechanical state on Earth. Heat flow studies [e.g., *Brune et al.*, 1969] have proposed that the fault stress inferred from surface heat flow data (i.e., ~20 MPa) is 5 times lower than that estimated by laboratory-derived values of rock friction (i.e., ~100 MPa) [*Byerlee*, 1978]. To resolve this issue, many have argued that the effective shear strength of the fault plane is weak [e.g., *Carpenter et al.*, 2011] and have suggested various weakening mechanisms, such as a reduction of the effective friction coefficient by thermal decomposition [*Han et al.*, 2007], melt formation by frictional heating [*Hirose and Shimamoto*, 2005], and a velocity-dependent friction coefficient [*Di Toro et al.*, 2004]. However, others have considered the case for strong fault planes. For instance, *Scholz* [2000] argued that stress rotation measurements in the Cajon Pass Scientific Borehole near the San Andreas Fault indicate that the fault is mechanically strong. The strong fault hypothesis requires a mechanism that masks the large amount of frictional heat along the fault plane. Even in the case of a weak fault, the reduction of shear strength may not be sufficient to explain completely the lack of positive heat flow anomalies.

[3] Although previous studies have successfully explained why faults are weak, they have focused only on the effective shear strength or the frictional coefficient [e.g., *Tembe et al.*, 2006]. On the other hand, the temperature- and pressure-dependent thermal conductivity, which plays an important role in the thermal evolution of the Earth [e.g., *van den Berg et al.*, 2004], has not been considered in analyses of observed surface heat flow data. Moreover, variable conductivity causes large heterogeneities in conductivity in the area surrounding the frictionally heated fault that may exert a nonnegligible influence on the surface heat flow. We carry out here numerical simulations to explore the relationship among variable thermal conductivity, frictional heating, and heat flow.

2. Numerical Model

[4] We employed a two-dimensional thermal-mechanical finite element code, Standard Us [*Hibbitt, Karlsson & Sorensen*, Inc. 2009], using ~500,000 elements with nonuniform gridding with the smallest resolution down to a few hundred meters. Figure 1 shows our model representing the uppermost part of the crust-lithosphere system. We predefine a narrow vertical rectangular fault with 10 km length and 2 km thickness. The center of the fault zone is placed at 12 km depth. The fault has a lower shear strength than the surrounding crust to localize shear/frictional heating. The fault is perpendicular to the direction of background deformation for strike-slip frictional motion. We assigned free surface at the top and a fixed in vertical direction boundary condition at the bottom. The right side of the domain has constant velocity boundary conditions (i.e., 3 cm/yr). The surface temperature is fixed at 300 K. The domain is warmed by a constant heat flux at the bottom boundary (i.e., 25 or 40 mW/m^2). After a steady geothermal gradient is achieved, the deformation for heat generation starts. We define two stages for deformation. The first stage is for deformation with shear/frictional heating on the predefined fault. Then, we terminate the deformation and let the fault cool down in the second stage in order to see the feature of thermal relaxation.

[5] The conservation of mass, momentum, and energy is described in the following equations:

[1]School of Earth and Environmental Sciences, Seoul National University, Seoul, South Korea.
[2]Minnesota Supercomputing Institute, University of Minnesota, Minneapolis, Minnesota, USA.
[3]Department of Earth Sciences, University of Minnesota, Minneapolis, Minnesota, USA.
[4]School of Environmental Sciences, China University of Geosciences, Wuhan, China.

Corresponding author: B.-D. So, School of Earth and Environmental Sciences, Seoul National University, Bldg. 25-1, Room 318a, Sillim-dong, Gwanak-gu, Seoul 151-742, South Korea. (qudekf1@snu.ac.kr)

0094-8276/13/10.1002/grl.50780

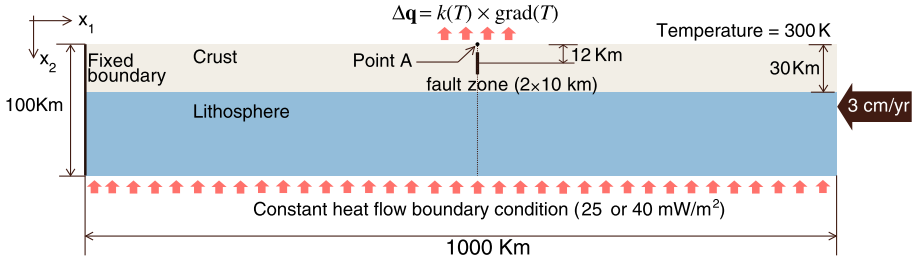

Figure 1. Schematic diagram of our model. The left and right vertical boundaries are thermally insulated. The red arrows above the fault in Figure 1 represent the surface heat flux **q**, which is decreased by the reduction of thermal conductivity $\Delta k(T)$ from frictional heating.

$$\frac{\partial v_i}{\partial x_i} = 0 \tag{1}$$

$$\frac{\partial \sigma_{ij}}{\partial x_j} = -\rho g_i, \left(\sigma_{ij} = -P\delta_{ij} + \tau_{ij}\right) \tag{2}$$

$$\rho c_P \frac{DT}{Dt} = \frac{\partial}{\partial x_i}\left(k\frac{\partial T}{\partial x_i}\right) + Q_s + Q_f. \tag{3}$$

[6] Additional explanations for the variables in the simulations can be found in Table 1. Total strain rate tensor can be simply described by the sum of elastic and plastic strain rates:

$$\dot{\varepsilon}_{ij}^{\text{total}} = \dot{\varepsilon}_{ij}^{\text{elastic}} + \dot{\varepsilon}_{ij}^{\text{plastic}} \tag{4}$$

where $\dot{\varepsilon}_{ij}^{\text{elastic}} = \frac{1}{2G}\frac{D\tau_{ij}}{Dt}$ (G = shear modulus). Q_s and Q_f in equation (3), respectively, indicate shear heating (i.e., $Q_s = \tau_{ij}\dot{\varepsilon}_{ij}^{\text{plastic}}$) and frictional heating following Byerlee's law [*Brace and Kohlstedt*, 1980]:

$$Q_f = (0.85\sigma_n)\dot{\varepsilon}_{12}^{\text{total}} \quad \sigma_n < 200 \text{ MPa} \tag{5}$$

$$Q_f = (0.6\sigma_n + 60 \text{ MPa})\dot{\varepsilon}_{12}^{\text{total}} \quad \sigma_n > 200 \text{ MPa},$$

where σ_n is the normal stress on the fault plane. Q_f is implemented only at fault planes under the assumption that the frictional sliding along the fault is perpendicular to the far-field compression throughout the lithospheric shortening.

[7] A Mohr-Coulomb yielding criterion with yield strength (σ_Y) is applied to determine strength of both layers [e.g., *Schmalholz et al.*, 2009]:

$$\tau^* \geq \sigma_Y, \tag{6}$$

where $\tau^* = \sqrt{0.25(\tau_{11} - \tau_{22})^2 + \tau_{12}^2}$ and $\sigma_Y = \sigma_n \sin\theta + C\cos\theta$. θ and C are the angle of internal friction and cohesion, respectively. The preexisting fault has zero cohesion. When the lithosphere satisfies the criterion (see equation (6)), the lithosphere behaves as a plastic flow with a temperature/deviatoric stress-dependent creeping law:

$$\dot{\varepsilon}_{ij}^{\text{plastic}} = AJ_2^{n-1}\tau_{ij}\exp\left(-\frac{E}{RT}\right). \tag{7}$$

[8] We apply laboratory-based rheological parameters of the crust [*Hansen and Carter*, 1983] and lithosphere [*Chopra and Paterson*, 1981] (see Table 1).

[9] Previous studies [e.g., *Hofmeister*, 1999] have determined that the thermal conductivity $k(T)$ varies as $(1/T)^b$:

$$k(T) = 1.7 \times (300/T)^b \text{ [W/m/K]}, (0 \leq b \leq 1). \tag{8}$$

[10] Although the thermal conductivity is also altered by pressure, the effect of temperature dominates over pressure dependence in the shallow crust [*Whittington et al.*, 2009]. The characteristic timescale of heat dissipation by conduction [*Gerya*, 2010] is derived from the length scale of the shear zone (i.e., 10 ~ 100 km) and heat diffusivity (i.e., 10^{-6} m^2/s). Since the characteristic timescale of heat dissipation by conduction is ~10 Myr, we calculate all models over a time span of 20 Myr.

3. Results

[11] We display results from numerical simulations that deal with the variations of conductivity that lead to the contrast in conductivity. In Figure 2, we exhibit the general features of the temperature profile along the dashed

Table 1. Input Parameters and Notations

Symbol	Values (Unit)	Descriptions
T		temperature
D/Dt		material derivative for temperature
		objective derivative for stress tensor
v_i		velocity in i direction
g_i		gravitational acceleration in i direction
σ_{ij}		stress tensor
τ_{ij}		deviatoric stress tensor
P	$-\frac{1}{2}(\sigma_{11} + \sigma_{22})$	pressure
δ_{ij}		Kronecker delta
J_2	$\frac{1}{2}(\tau_{ij}\tau_{ij})^{1/2}$	second invariant of τ_{ij}
ν	0.3	Poisson's ratio
ρ	3000 (kg/m^3)	density
G	10^{11} (Pa)	shear modulus
c_P	900 (J/(kg · K)]	specific heat
R	8.314 (J/(K/mol))	universal gas constant
θ_s	30°	angle of internal friction of the domain
C_s	10 (MPa)	cohesion of the domain
θ_f	30°	angle of internal friction of the fault
C_f	0 (MPa)	cohesion of the fault
E_c	190 (kJ/mol)	activation energy of crust
n_c	3.3	power law exponent of crust
A_c	3.16×10^{-26} (Pa^{-n} · s^{-1})	prefactor of crust
E_{litho}	498 (kJ/mol)	activation energy of lithosphere
n_{litho}	4.48	power law exponent of lithosphere
A_{litho}	5.5×10^{-25} (Pa^{-n} · s^{-1})	prefactor of crust of the lithosphere

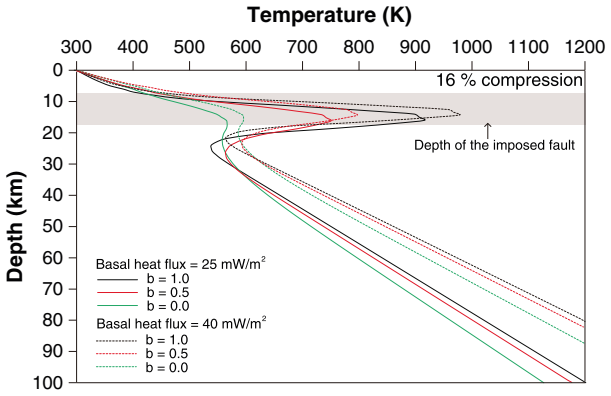

Figure 2. Temperature profiles for varying values of b at 16% compression with 25 and 40 mW/m^2 basal heat flux conditions. The gray shaded area indicates depth range of the imposed fault. The large value of b reinforces frictional/shear heating by suppressing heat diffusion.

line (see Figure 1) for cases of $b = 0$, 0.5, and 1 with basal heat fluxes of 25 and 40 mW/m^2. At the stage where 16% compression has been attained, we can observe localized thermal instabilities around the fault due to frictional/shear heating. The temperatures around the zone are much higher for larger values of b than for smaller values of b. Moreover, the temperature profile is most localized for $b = 1$. Although both cases with different basal heat fluxes show similar results, the geothermal gradient in the case of lower basal heat flux is gentler.

[12] Figures 3a and 3b show profiles of the vertical heat flux, which refers to the vertical component of the heat flux vector, and conductivity to explain the relationship between weak heat flow anomalies and the thermal insulator. We also tested the effect of different values of the background heat flow (i.e., basal heat flux boundary conditions of 25 and 40 mW/m^2). Figure 3a shows heat flux profiles along the vertical line across the center of the domain (see the dashed line in Figure 1) for basal heat fluxes of 25 mW/m^2 (solid lines) and 40 mW/m^2 (dashed lines). Although the general features are similar for both basal heat fluxes, the magnitudes of the heat fluxes are higher in the case of the 40 mW/m^2 basal heat flux. To account for the insulating effect of the conductivity contrasts, we show thermal conductivity profiles along the dashed line (see Figure 1) at 16% compression (Figure 3b). The maximum contrast in conductivity between the hot fault and the cold surface is a factor of 3 in the case of $b = 1$ (see the black line in Figure 3b).

[13] Lower values of b create weaker frictional heating and broader temperature distributions (see Figure 2). However, in Figure 3a, lower values of b result in more efficient heat conduction. This phenomenon may suggest an alternative hypothesis to partially explain the lack of heat flux anomalies near faults. We speculate that this contrast may retard the diffusion of heat toward the cold region. On the other hand, there is no contrast in conductivity in the case of $b = 0$. In this case, the heat can diffuse effectively. Heat diffusion is detected clearly by surface heat flow because of the absence of any thermal insulator (see the green line in Figure 3b).

[14] To follow the time histories of the surface heat flux at Point A (see Figure 1), we defined two stages for Figure 4a. The first stage includes constant deformation rate that leads to frictional heating on the predefined fault. In the second stage, we terminate the deformation to stop the generation of heat and observe how the heat flux relaxes. As discussed previously, a higher value of b results in weaker surface heat flux even though this case contains a much warmer localized zone (see Figure 2). In this case, there can be a strong contrast in thermal conductivity, which cannot occur in the case of constant conductivity (i.e., $b = 0$). In the second stage, the heat flux decreases because of the diffusion of the localized heat. The case of $b = 1$ shows the small variation in surface heat flux with time. Thus, we may infer that a thermal insulator is present between the warm fault and the cold surrounding crust. Moreover, a large time lag between the termination of deformation and temperature drop in the case of $b = 1$ indicates the existence of a strong thermal insulator (see Figure 4a). On the other hand, the case of $b = 0$ depicts the fastest increase and relaxation of the heat flux after the termination of deformation.

[15] In order to check the energy conservation in our numerical models, we plot the time-integrated release of heat along the surface (Figure 4b). The total energy generated by shear/frictional heating, ~3.7×10^5 TJ (see the dashed arrow in Figure 4b), is gained from the integration of surface heat flux along the surface (i.e., 1000 km) and time (i.e., 6.6 Myr). Then, the total energy is divided by the area of the place where shear/frictional heating occurs (i.e., ~100 km^2). This corresponds to the heat generation rate, ~20 μW/m^2, which is similar with the shear heating rate in previous studies [e.g., *Gerya et al.*, 2004]. All models

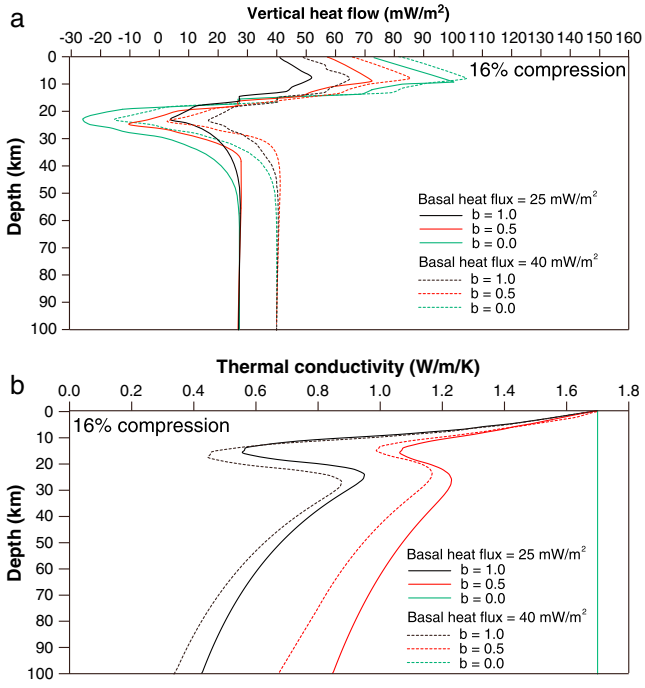

Figure 3. (a) Heat flux profiles along the dashed line (see Figure 1) with varying values of b for cases of 25 mW/m^2 (solid lines) and 40 mW/m^2 (dashed lines) basal heat fluxes. Both cases show weak heat flux in the case where $b = 1$. (b) Conductivity profiles along the dashed line in Figure 1 with varying values of b. There is a clear conductivity contrast in the case of $b = 1$. This contrast in conductivity acts as a thermal insulator.

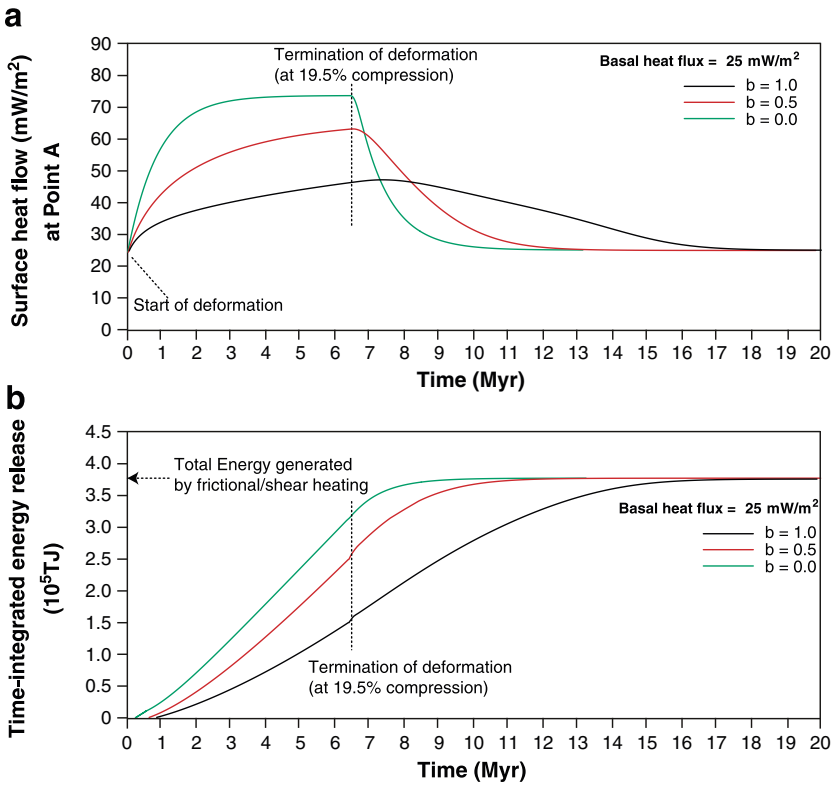

Figure 4. (a) Temporal evolutions of the vertical heat flux with varying values of b observed at Point A (see Figure 1). When $b = 1$, the heat flux is weakest (50% less than the case of $b = 0$) and the least sensitive to frictional heating. (b) Time-integrated energy release along the surface. All models release almost the same level of heat generated by friction and shear heating. This means that our model confirms energy conservation.

release almost the same energy because the amount of deformation and initial strength are similar in all models. Thus, we can conclude that the energy is conserved in our runs. However, the case of $b = 1.0$ releases the heat very slowly compared with the case of $b = 0$.

[16] Although initial geothermal gradients with varying b values are different and then cause a different distribution of rheological properties through the temperature-dependence in the plastic strength, the strength around the fault is almost the same because it exists in the shallow part of the crust (depth from 5 to 15 km). On the other hand, a deeper part, which has large temperature difference with varying b values, is difficult to be yielded plastically due to a large pressure. This means that the part far from the fault hardly generates shear heating and all thermal energy comes from the region around the imposed fault. Thus, all models with different b values generate a similar level of thermal energy.

4. Discussion

[17] We calculated the time histories of both temperature and heat flow for different values of thermal conductivity. Generally, the thermal structure and heat transport are dictated by the competing interaction between frictional heating and heat diffusion. However, the particular value of b in $k(T)$ determines the dominant effect. If the conductivity decreases with increasing temperature, this decrease suppresses the diffusion of heat from the fault zone to the surrounding crust. Thus, the temperature near the fault is much higher with variable conductivity than in the uniform conductivity case. Consequently, a significantly large conductivity contrast is induced in all models except for the case of constant thermal conductivity. When $b = 1$, conductivity contrasts of 3 are produced at a compression of 16%. For the case of $b = 1$, the surface heat flow is less than half of that with constant thermal conductivity. Moreover, the contrast impacts the evolution of surface heat flow. In the case of constant conductivity, the heat flow increases rapidly with frictional heating and relaxes quickly after the deformation ceases.

[18] The thermal conductivity contrast has two important implications in explaining the weak heat flow anomalies near faults. First, it is the contrast of conductivity which is responsible for the insulation of the heat produced near the fault. We observed that the heat flux is weak and insensitive to time in spite of the large amount of heat around the fault when there is a conductivity contrast. This result implies that the contrast can cause a thermal insulating effect within the localized region. Vertical heat transport from the localized zone is restricted, and the surface heat flow anomaly remains undetectably low. Unless a comprehensive analysis of the variations in conductivity with temperature and its contrast is performed, the observed heat flow data cannot provide accurate information about the thermal state within the crust near faults.

[19] Second, the mechanical strength of the fault can effectively be reduced by the pronounced frictional heating due to the insulating effect in the case of variable conductivity. Many laboratory experiments have shown that strength is significantly affected by increases in temperature. For instance, higher temperatures due to significant heating

enhances rock melting [*Kanamori et al*., 1998] and thermal decomposition [*Han et al*., 2007], which are important mechanisms in reducing the strength of fault rock. The variable conductivity case in this study also resulted in much higher temperature (~400 K) with sufficient deformation (i.e., 16%). Thus, we suggest that the variable conductivity causes a larger reduction of the effective strength within the localized friction zone. A friction model with variable conductivity may better explain the reduction of shear strength than one with constant conductivity. In brief, our hypothesis gives a simple idea that strongly temperature-dependent conductivity plays a nonnegligible role in causing low surface heat flow anomalies along faults because of the insulation effect and the enhanced reduction of fault rock strength.

[20] Furthermore, we need to include more realistic mechanisms in the model, such as a temperature-induced weakening rheology [e.g., *Hirose and Shimamoto*, 2005; *Han et al*., 2007] and advective heat transport [e.g., *Smith and Chapman*, 1983]. If the reduction in shear strength from frictional heating interplays with the variable conductivity, the feedback between frictional heating, surface heat flux, and strength reduction may be more complicated. Heating with variable conductivity and a temperature-induced strength weakening mechanism cause two competing effects of strength reduction and the broadening of the conductivity contrast. The former effect decreases the surface heat flux because of low frictional heat generation, while the latter increases the heat flux. In addition, heat transport by fluid convection also disturbs and redistributes the surface heat flux and the heat source. Rather than excluding these possibilities, we propose that the insulating effect may be consistent with previous hypotheses. An additional question is if this insulation hypothesis also works when rock is melted by frictional heating [*Kanamori et al*., 1998]. We estimated a 400 K higher temperature around the fault zone in the case of variable conductivity (i.e., $b = 1$). This could cause melting along the fault plane, which has been thought to be an important factor for the slip rate and heat transport of faults [e.g., *McKenzie and Brune*, 1972]. Because melted rocks generally have lower conductivities than crystalline rocks [*Pertermann et al*., 2008], the existence of melts on the fault plane may reduce the surface heat flux due to an intensification of the thermal insulation and the weakening shear strength around the fault plane.

5. Conclusions

[21] Our approach in investigating the lack of positive heat flow anomalies along major faults is fundamentally different from previous studies that were based on only the shear strength of the fault rocks. Several authors have suggested different mechanisms, such as rolling grains [*Mora and Place*, 1998] and the reduction of normal stress by fault interface vibration [*Brune et al*., 1993], to avoid strength weakening mechanisms. The thermal insulating effect in this study is consistent with the above hypotheses. Strong insulation, which is caused by the positive feedback between frictional heating and the dramatic reduction in the thermal conductivity, may provide a partial explanation for the heat flow constraint.

[22] **Acknowledgments.** This work was supported by the Korean government (MEST, 2009-0092790) for B.-D. So and by the U.S. National Science Foundation grants in the Collaboration of Mathematics and Geosciences (CMG) program and Geochemistry for D. A. Yuen.

[23] The Editor thanks Masanori Kameyama and Stefan Schmalholz for assistance in evaluating this paper.

References

Brace, W. F., and D. L. Kohlstedt (1980), Limits on lithospheric stress imposed by laboratory experiments, *J. Geophys. Res.*, *85*, 6248–6252.

Brune, J. N., T. L. Henyey, and R. F. Roy (1969), Heat flow, stress, and rate of slip along the San Andreas Fault, California, *J. Geophys. Res.*, *74*(15), 3821–3827.

Brune, J. N., S. Brown, and R. A. Johnson (1993), Rupture mechanism and interface separation in foam rubber models of earthquakes: A possible solution to the heat flow paradox and the paradox of large overthrusts, *Tectonophyscis*, *218*(1–3), 59–67.

Byerlee, J. D. (1978), Friction of rock, *Pure Appl. Geophys.*, *116*(4–5), 615–626.

Carpenter, B. M., C. Marone, and D. M. Saffer (2011), Weakness of the San Andreas Fault revealed by samples from the active fault zone, *Nat. Geosci.*, *4*, 251–254.

Chopra, P. N., and M. S. Paterson (1981), The experimental deformation of dunite, *Tectonophysics*, *78*(1–4), 453–473.

Di Toro, G., D. L. Golbsby, and T. E. Tullis (2004), Friction falls toward zero in quartz rock as slip velocity approaches seismic rates, *Nature*, *427*, 436–439.

Gerya, T. V. (2010), *Introduction to Numerical Geodynamic Modelling*, Cambridge University Press, Cambridge, UK, pp. 345 .

Gerya, T. V., D. A. Yuen, and W. V. Maresch (2004), Thermo-mechanical modelling of slab detachment, *Earth Planet. Sci. Lett.*, *226*(1–2), 101–116.

Han, R., T. Shimamoto, T. Hirose, J.-H. Ree, and J.-i. Ando (2007), Ultralow friction of carbonate faults caused by thermal decomposition, *Science*, *316*(5826), 878–881.

Hansen, F. D., and N. L. Carter (1983), Semibrittle creep of dry and wet Westerly granite at 1000 MPa, in *The 24th US Symposium on Rock Mechanics*, pp. 429–447, Texas A and M University, College Station, Texas.

Hibbitt, Karlsson & Sorensen, Inc. (2009), Abaqus/Standard User's Manual Version 6.9, Pawtucket, RI.

Hirose, T., and T. Shimamoto (2005), Growth of molten zone as a mechanism of slip weakening of simulated faults in gabbro during frictional melting, *J. Geophys. Res.*, *110*, B05202, doi:10.1029/2004JB003207.

Hofmeister, A. M. (1999), Mantle values of thermal conductivity and the geotherm from phonon lifetimes, *Science*, *283*(5408), 1699–1706.

Kanamori, H., D. L. Anderson, and T. H. Heaton (1998), Frictional melting during the rupture of the 1994 Bolivian earthquake, *Science*, *279*(5352), 839–842.

McKenzie, D., and J. N. Brune (1972), Melting on fault planes during large earthquakes, *Geophys. J. Int.*, *29*(1), 65–78.

Mora, P., and D. Place (1998), Numerical simulation of earthquake faults with gouge: Toward a comprehensive explanation for the heat flow paradox, *J. Geophys. Res.*, *103*(B9), 21,067–21,089.

Pertermann, M., A. G. Whittington, A. M. Hofmeister, F. J. Spera, and J. Zayak (2008), Transport properties of low-sanidine single crystals, glasses and melts at high temperature, *Contrib. Mineral. Petrol.*, *155*, 689–702, doi:10.1007/s00410-007-0265-x.

Schmalholz, S. M., B. Kaus, and J.-P. Burg (2009), Stress-strength relationship in the lithosphere during continental collision, *Geology*, *37*(9), 775–778.

Scholz, C. H. (2000), Evidence for a strong San Andreas fault, *Geology*, *28*(2), 163–166.

Smith, L., and D. S. Chapman (1983), On the thermal effects of groundwater flow: 1. Regional scale systems, *J. Geophys. Res.*, *88*(B1), 593–608.

Tembe, S., D. A. Lockner, J. G. Solum, C. A. Morrow, T.-F. Wong, and D. E. Moore (2006), Frictional strength of cuttings and core from SAFOD drillhole phases 1 and 2, *Geophys. Res. Lett.*, *33*, L23307, doi:10.1029/2006GL027626.

Whittington, A. G., A. M. Hofmeister, and P. I. Nabelek (2009), Temperature-dependent thermal diffusivity of the Earth's crust and implications for magmatism, *Nature*, *458*, 319–321.

van den Berg, A. P., D. A. Yuen, and E. S. G. Rainey (2004), The influence of variable viscosity on delayed cooling due to variable thermal conductivity, *Phys. Earth Planet. Inter.*, *142*, 283–295.